SLURRY PHASE IRON CATALYSTS FOR INDIRECT COAL LIQUEFACTION

Contract No. DE-FG22-95PC95210

to DOE/PC/95210--T2

The University of New Mexico

7/5/95 - 7/4/98

Second Semi-Annual Progress Report

Covering the Period from 1/5/96 - 7/4/96

Prepared for

U. S. Department of Energy
Pittsburgh Energy Technology Center
PETC Project Manager: Richard E. Tischer

Submitted by

Abhaya K. Datye, Professor
Department of Chemical & Nuclear Engineering and
Director, Center for Microengineered Materials
University of New Mexico
Albuquerque, NM 87131

August 2, 1996

Executive Summary

This report covers the second six months of this three year grant under the University Coal Research program. During this period we have continued our work on understanding the attrition of precipitated iron catalysts and initiated work on synthesis of catalysts containing silica binders. As we show in this report, the use of a sedigraph particle size analyzer with an ultrasonic probe provides a simple method to test the strength of catalyst agglomerates. This approach allows us to compare the relative strength of a silica support and the hematite catalyst obtained from the Laporte run II. The silica support is considerably stronger than the hematite catalyst. In future work, we will use this approach to study the role of binders in influencing the strength of the precipitated catalysts.

During this period, we have continued our study of Fe/silica interactions to provide a fundamental understanding of the how silica binders influence the activity and attrition resistance of these catalysts. In our previous report we had shown how an unreducible silicate-like phase was observed when the $Fe(NO_3)_2$ was co-precipitated with a tetraethylorthosilicate (TEOS) precursor. Based on the suggestion made by Dr Tischer, the project manager, we used a colloidal silica precursor and added it to the calcined Fe_2O_3 catalyst. There was no detrimental effect on the reducibility of the hematite to α-Fe. We also studied a catalyst containing 30% Fe supported on silica and found that it does not reduce to α-Fe as quickly as an unsupported catalyst. But this is a kinetic effect and longer reduction periods allow complete reduction of the Fe_2O_3 to α-Fe. No silicate phase is seen to form at temperatures used in this study (<723K). In future we will study the role of oxidation-reduction treatments on the Fe-silica interaction. The oxidation-reduction conditions will be similar to those encountered in a bubble column reactor during Fischer-Tropsch synthesis.

In May of 1996, we received a set of samples from Dr. Burtron Davis from a Fischer-Tropsch run lasting over 3000 hours. During this run, samples were obtained at various times. The samples are embedded in wax and therefore not subject to oxidation by the ambient atmosphere. A similar set of samples for a number of runs have also been received from Dr. Dragomir Bukur. Of these we have selected one run for in-depth study. These analyses should allow us to observe the phase evolution as a function of time on stream. Such analyses have previously been performed by Mossbauer spectroscopy at the University of Kentucky. Our objective here is to use a combination of X-ray diffraction and electron microscopy to map out the size distribution of the crystalline phases and the types of carbon present in these samples. The major difficulty in the use of x-ray diffraction is that the magnetite and carbide peaks overlap, making it difficult to properly assess the relative amounts of these phases. As we show in this report, we have developed an approach based on Reitveld refinement that allows us to separate the carbide and magnetite peaks. We will use this approach to complete the XRD analyses of these wax embedded samples.

Technical Objectives

This objective of this research project is to perform fundamental research in support of catalyst development for slurry phase bubble column reactors for Fischer-Tropsch synthesis. The overall program is divided into the following tasks:

Task 1. Catalyst Particulate Synthesis
Task 2. Catalyst Binder Interactions.

In task 1, we will first study factors that determine the attrition resistance of slurry phase Fe catalysts. Fundamental understanding of the attrition phenomenon will be used to guide the synthesis of novel precipitated catalysts that overcome some of the limitations of current generation catalysts. The investigation of catalyst microstructure as a function of treatment will help determine the optimal treatment protocols for F-T synthesis catalysts. Since the use of binders is considered essential for providing the desired attrition resistance, the second task is to perform fundamental studies of catalyst-binder interactions. These studies will use model catalysts that can be studied by high resolution transmission microscopy to investigate the nature of interfacial phases at the Fe-binder interface. A better understanding of the phenomena that lead to catalyst-binder interactions can lead to the design of improved catalysts indirect coal liquefaction.

Task 3. Characterization of catalysts received from Univ. of Kentucky and from Texas A&M

Task 3 was not included in our original proposal. However, we are pursuing these studies to help understand catalyst deactivation under actual reaction conditions.

Technical Progress
Task 1: Catalyst Particulate Synthesis

Attrition of precipitated Fe catalysts

Our preliminary work published in Appl. Catal. last year showed that a sedigraph particle analyzer coupled with an ultrasonic probe can yield a simple test for the strength of catalyst agglomerates. During this six month period we have continued work on this method to examine whether it can be used to derive a quantitative estimate of agglomerate strength. I have attached a detailed report of this work in the form of an appendix. The salient results will be summarized here. Figure 1 shows a plot of particle size distribution for a Davisil silica sample subjected to ultrasound using a Tekmar probe at setting 5. As seen from this plot, the silica particles break down with increasing exposure to ultrasound. Based on the approach outlined in the appendix, we can work out a breaking strength for the silica particulates of 1130 psi. At the same setting, the kaolin binder-containing UCI catalyst was found to break down completely into its primary particles within a minute. Its breaking strength on the same scale is estimated to be 1-3 psi.

The role of binder morphology

Examination of the particle break down occurring with the kaolin-binder catalyst suggests that the binder plays a minimal role in increasing particulate strength. This can be seen in Fig. 3 where the breakdown of the base UCI catalyst 1185-149 is compared with the binder containing catalyst (UCI 1185-75-370). The poor performance of the kaolin binder can be attributed to its morphology, thin sheets that are of μm size but with smooth surfaces. Examining the primary hematite crystallites suggests that a rougher, more fractal morphology would be more suitable for providing particulate strength. To this end, we have commenced studies of various silica binder morphologies to evaluate the role of morphology on particle strength. The first sample we have prepared involves the deposition of colloidal silica on the primary particles of the UCI catalyst 1185-149. These particles were obtained by sonicating the base catalyst to break down the aggregates. Fig. 4 shows a TEM image of the colloidal silica deposited on the hematite crystals after calcination at 300 °C. This sample was calcined at temperatures up to 800 °C to determine the temperature at which the silica would sinter and form a uniform coating on the hematite surface. We found that the silica did not sinter much at these temperatures, however the hematite did start to sinter at temperatures above 650 °C, so we will restrict the calcination temperature to 600 °C in future work. Alternate silica morphologies can be obtained by varying the silica precipitation conditions. Fig. 5a shows silica deposited via precipitation from sodium silicate solutions. This yields a more silica particles with a more fractal morphology and these particles stick nicely to the hematite crystals. As shown in Fig. 5b, we do find the silica precipitating often between hematite crystallites. Having silica particles bridge the hematite crystals may provide better strengthening of the agglomerates.

Future Work

The next phase of this work is to test the strength of the silica binder containing agglomerates. Since it is difficult to spray dry small batches of catalyst, we have chosen to form aggregates of these powders simply via drying and calcination of the powders. These powders will be sieved and the particles in the 30-100 μm range will be tested using ultrasonic fragmentation.

Task 2 - Catalyst-binder interaction

The objective of the study is to determine the nature of interfacial phases formed, if any, when silica is deposited in Fe or vice-versa. For these experiments we examined two types of samples:

a) Colloidal silica deposited on the primary particles derived from UCI 1185-149 to yield 20% silica by weight on the base catalyst (shown in Fig. 4).

b) $Fe(NO_3)_2$ impregnated on silica at a weight loading of 10, 20 and 30% Fe/SiO_2. In these catalysts, $Cu(NO_3)_2$ was added to the mixture to improve reducibility. The overall composition of the catalyst was Cu/Fe=0.05; K/Fe=0.06 by weight.

The reduction of these catalysts in flowing H_2 at 450 °C was performed and the catalysts analyzed by XRD and TEM. Fig. 6 shows the x-ray diffraction pattern of the UCI 1175-149 catalyst reduced in H_2 for 2 hours. The catalyst shows a small magnetite peak, a Cu peak indicating the Cu has phase segregated to form metallic islands of Cu, and a prominent α-Fe peak. The UCI catalyst with 20% colloidal silica deposited on it was studied next (this catalyst was shown in Fig. 4). The x-ray diffraction powder pattern (Fig. 7) shows no effect of silica on the reduction of the Fe_2O_3 to α-Fe.

Similar observations were made with the 30% Fe/SiO_2 gel impregnated catalyst. Fig. 8 shows an XRD powder pattern of the 30% Fe/SiO_2 catalyst after reduction at 450 °C for 2 hours. The magnetite peak is more pronounced than in Fig. 6 indicating that impregnating Fe on silica makes it harder to reduce. However, this is more of a kinetic limitation since overnight reduction seems to allow complete reduction to α-Fe as shown in Fig. 9. The reduction of these catalysts by CO was also studied using temperature programmed reduction (shown in Fig. 10). While the reduction peaks are better defined in the unsupported UCI catalyst, qualitatively the reduction profiles are similar.

In summary, when colloidal silica is deposited on the precipitated iron catalyst, we do not observe any silicate phases or any influence of the silica on the reducibility of Fe_2O_3. On the other hand, when $Fe(NO_3)_2$ is impregnated on silica gel, we find that 2 hr reduction in H_2 does not permit complete reduction to α-Fe. However, the reduction is complete after overnight reduction and there is no unreduced magnetite left in the sample. No silicate phase was observed by x-ray diffraction.

Future Work

In future work, we will study the effect of calcination at higher temperatures to determine under what conditions the iron silicate phase will form and the extent to which silicate formation hinders the reducibility of the Fe_2O_3. We will also subject the reduced Fe catalyst to oxidation-reduction cycles to see if silicate formation (and the production of unreducible Fe) occurs under conditions encountered during F-T synthesis.

Task-3: Characterization of catalysts from Univ. of Kentucky & Texas A&M

As mentioned in our previous progress report, careful passivation of these catalysts is essential to preserving the microstructure and phase composition of these catalysts. While we are working on techniques that lead to more controlled passivation of these catalysts, at present we have decided to restrict our study to

catalysts that are embedded in the waxy hydrocarbons during removal from the reactor.

Fig. 11 shows an XRD powder pattern for a sample obtained from run SB-3425 at TOS=0 hr from Dr. Bukur. The pattern shows prominent α-Fe peaks with just a hint of magnetite. We can therefore conclude that the sample must have been reduced to metallic Fe and is well preserved in the hydrocarbon oil. This result show that the sample microstructure is quite well preserved in this catalysts and surface oxidation does not occur.

Fig. 12 shows an XRD powder pattern from a sample obtained from Dr. Burt Davis, from run RJO189P. This sample was removed from the reactor after 3547 hours of reaction. Three plots are included in this pattern, YOBS the raw data, YCALCZ the calculated pattern for magnetite that best fits the data using a Reitveld analysis procedure and YDIFF the difference plot. The method used, Reitveld analysis, is a non linear regression procedure that provides the best fit of the data to a given structure, in this case magnetite. After fitting the magnetite, the residual represents the other phases present in the catalyst. As shown here, this procedure allows us to accurately quantify the amount of iron carbide and other phases that may be present in this sample. In Fig. 13, we show an application of the same procedure but after inclusion of the magnetite as well as Cu. One of the carbide peaks has the same d values as Cu(111), however the residual plot now shows negative peaks corresponding to the other Cu lines that are missing in the XRD pattern. Hence, we can rule out the presence of a separate Cu phase in this catalyst unlike the UCI 1185-149 catalyst where we do see free Cu after H_2 reduction.

One major concern with x-ray diffraction analysis is the possibility of preferred orientations. If the sample has preferred orientations, the ratios of peaks could be altered making it difficult to perform quantitative analysis. In our case, with the catalyst being suspended in a wax slurry minimizes the possibility of preferred orientation effects.

The suitability of the Reitveld analysis was tested by performing the analysis of a sample of natural magnetite. These results are shown in Fig. 14. The observed data and the calculated profile are in excellent agreement such that the residual plot shows no other phase being present.

Fig. 15 shows the residual plot for sample RJO189P indicating the x-ray diffraction pattern of the carbide phase. This plot confirms the presence of a substantial amount of carbide in the sample after 3547 hours on stream in a F-T slurry reactor.

Future Work

In future work, we will continue analysis of the samples obtained from Drs Bukur and Davis to complete the determination of the phases present in an F-T reactor as

function of time. This will provide definitive data on the nature of the active phase in these catalysts and the causes of catalyst deactivation.

Acknowledgments

The following graduate and undergraduate students participated in this project: Linda Mansker, x-ray diffraction; Yaming Jin, F-T reactor studies; Aree Hanprasopwattana - catalyst synthesis and surface coatings; John Reardon - attrition resistance studies; Steven Medd - summer NSF/REU student working on silica strengthening mechanisms; Juan Ray Griego - summer ORISE student working on Fe/silica interaction studies. We also acknowledge helpful discussions with Dr. Mark Miller of the Earth and Planetary Sciences on Reitveld refinement methods for analysis of x-ray diffraction patterns. The TEM and XRD measurements were performed using the analytical facilities provided by the Earth and Planetary Sciences Department.

Figure Captions

Fig. 1 Sedigraph particle size distributions as a function of ultrasound treatment for Davisil silica. The fraction of fine particles is seen to increase as a result of particle breakdown. The failure of the baseline to go to zero implies that particles finer than 0.2 μm are being produced during ultrasonication.

Fig. 2 Particle breakdown caused by ultrasonication of kaolin binder containing UCI catalyst. The agglomerates are broken down much quicker than the silica particles shown in Fig. 1.

Fig. 3 Comparison of the breakdown of the binderless catalyst with the kaolin binder containing UCI catalysts. The kaolin binder does not impart any additional strength to the catalyst.

Fig. 4 Colloidal silica deposited on primary particles derived from UCI catalyst 1185-149. The silica is present in the form of spherical particles that cover the surface of the hematite quite uniformly.

Fig. 5a Silica precipitated from sodium silicate on to the primary particles derived from UCI catalyst 1185-149. The silica is present in the form of fractal aggregates that stick very well to the hematite.

Fig. 5b In many cases, the precipitated silica is seen to bridge hematite crystals.

Fig. 6 XRD powder pattern of UCI base catalyst 1185-149 reduced in H_2 at 450 °C for 2 hours.

Fig. 7 XRD powder pattern of UCI base catalyst on which 20% colloidal silica had been deposited (see fig. 4 for a TEM of this catalyst) after reduction in H_2 at 450

°C for 2 hours. The presence of silica on the surface does not inhibit reduction of the silica.

Fig. 8 XRD powder pattern of 30% Fe on silica gel, reduced in H_2 at 450C for 2 hours. The reduction to α-Fe is incomplete.

Fig. 9 XRD powder pattern of 30% Fe on silica gel after overnight reduction in H_2 at 450 °C. Reduction to α-Fe is now complete and no inhibition by silica is observed.

Fig. 10 Temperature programmed reduction of the UCI catalyst 1185-149 and the 30% Fe/silica gel catalyst in flowing CO. Some of the distinct reduction peaks seen with the unsupported catalyst are missing on the supported catalyst and the reduction peak maximum has shifted to higher temperatures.

Fig. 11 XRD powder pattern of sample SB-3425 embedded in wax, after 0 hours on stream. A prominent α-Fe peak is seen with a small magnetite peak.

Fig. 12 XRD powder pattern of sample RJO189P embedded in wax. The three plots shown represent the raw data, the calculated best fit for magnetite and the residual. The residual plot clearly shows substantial amounts of iron carbide still present after 3547 hours on stream.

Fig. 13 XRD powder pattern of the same sample RJO189P shown in fig. 12. This time the calculated plot is the best fit for magnetite as well as metallic Cu being present. The 1.828 Å Cu peak is clearly absent as indicated by the negative peak in the difference pattern. Hence, the 2.195 Å peak can be assigned to the carbide rather than to Cu(111).

Fig. 14 XRD powder pattern of natural magnetite along with the calculated pattern based on a Reitveld refinement. The difference pattern shows clearly the absence of any other phases and indicates the utility of the Reitveld refinement approach for separating the magnetite and carbide peaks in the samples removed from the reactor.

Fig. 15 The carbide XRD powder pattern from sample RJO189P. The peak at 20° 2θ arises due to the wax. The prominent carbide reflections are at 2.037 Å and at 2.110Å with a smaller peak at 2.199 Å. There are other peaks at higher values of 2θ which taken together should allow us to perform a Reitveld refinement of the carbide structure.

Fragmentation of Davisil silica

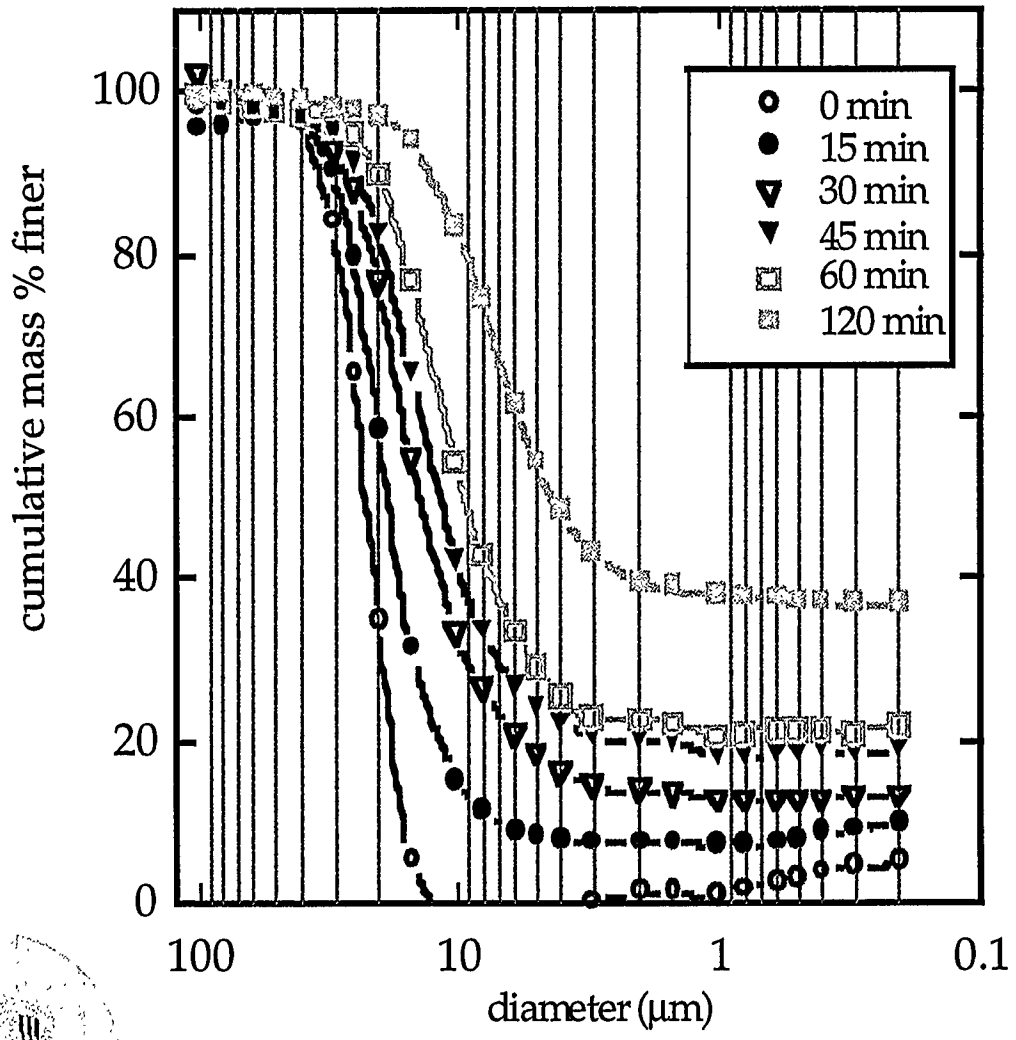

Setting N=5
ε=9.64 W
P_c=3312 psia
(228 bar).

UNM

Fig. 1

Fragmentation of Hematite-Kaolin catalyst

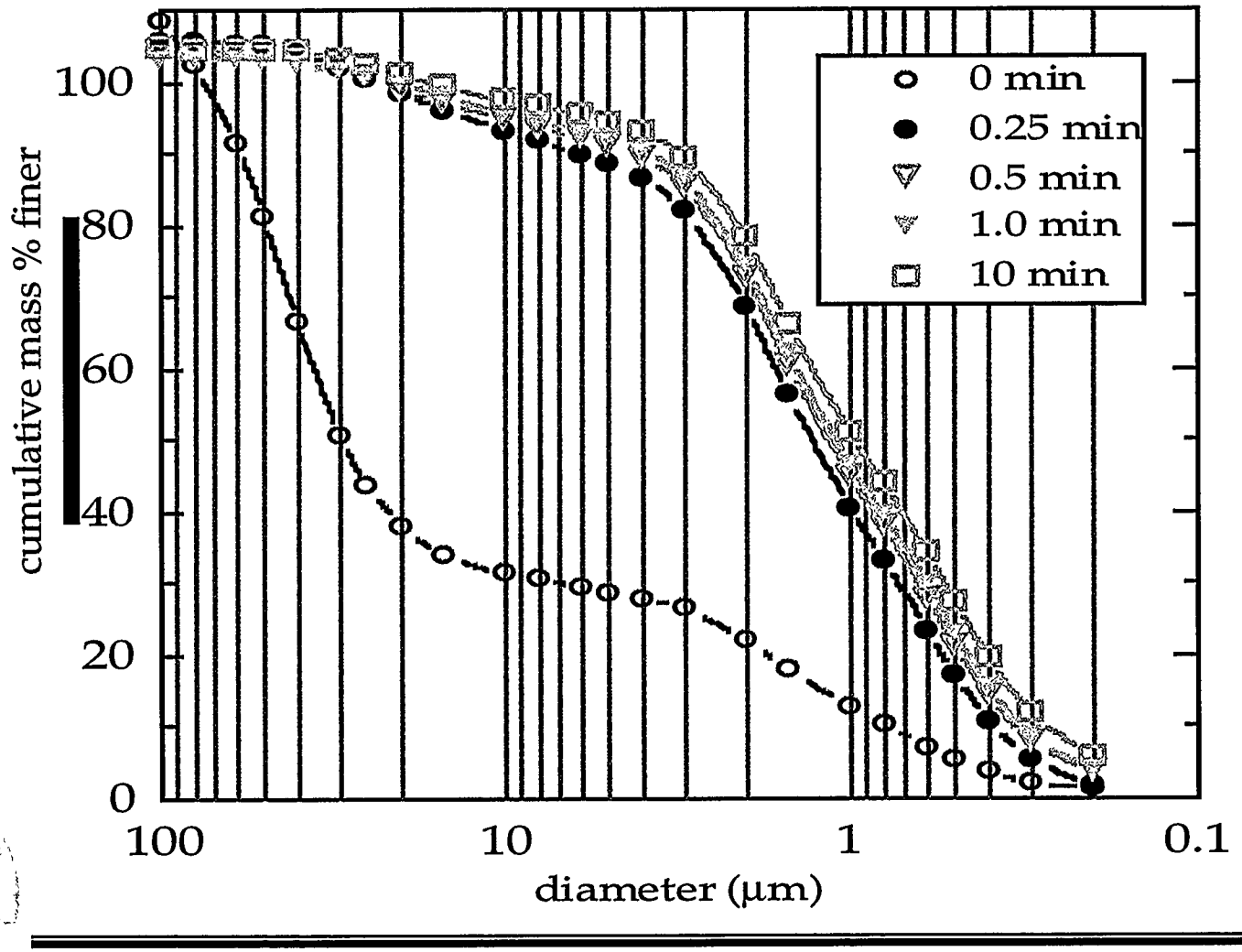

Setting
N=5

UNM

Fig. 2

Effect of Kaolin(K) binder on fragmentation of Hematite(H)

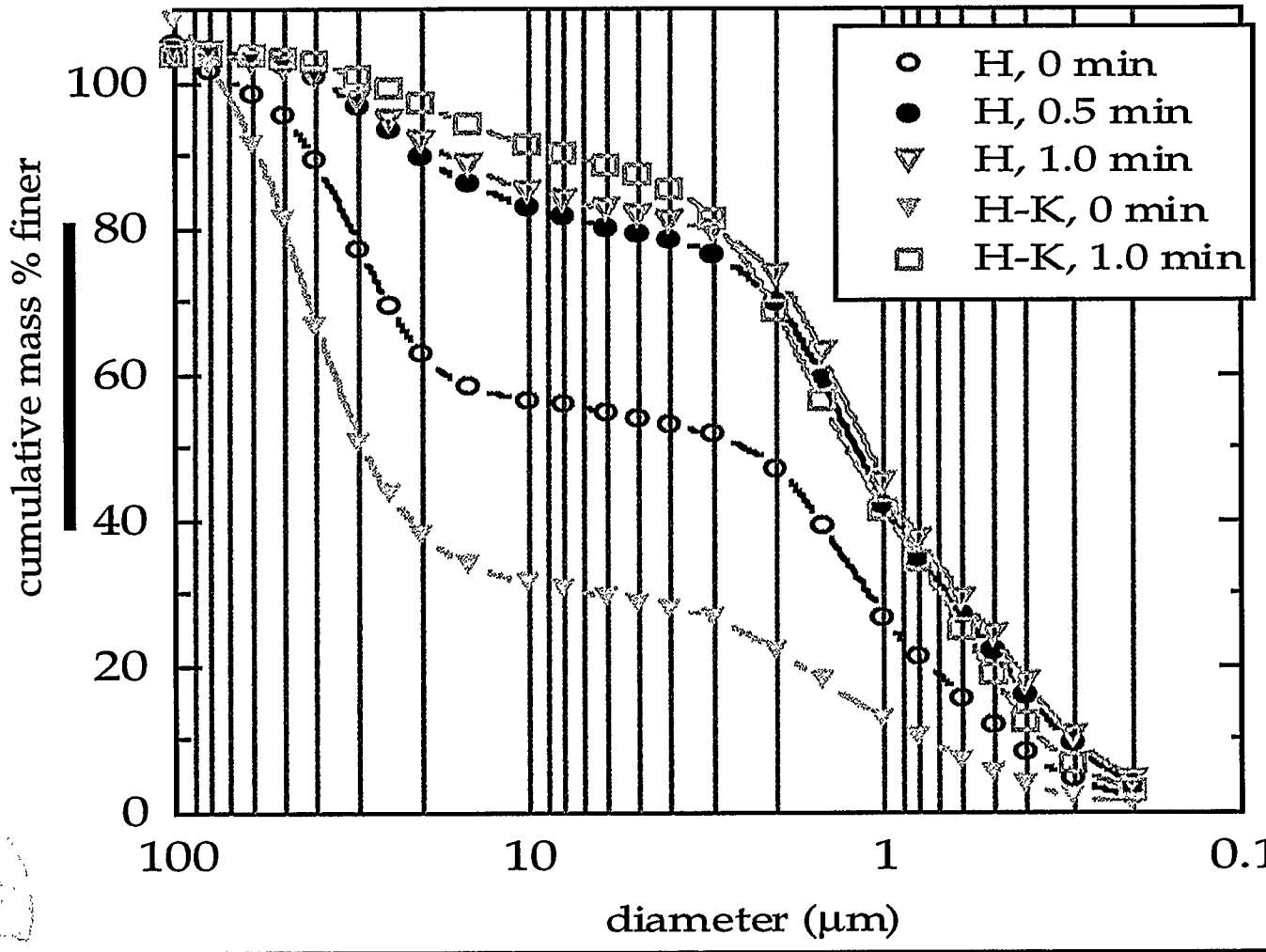

Setting
N=2
e=2.07 W
Pc=346 psia
(23.9 bar)

UNM

Fig. 3

Base catalyst plus colloidal silica calcined at 300°C for 3.5 hours

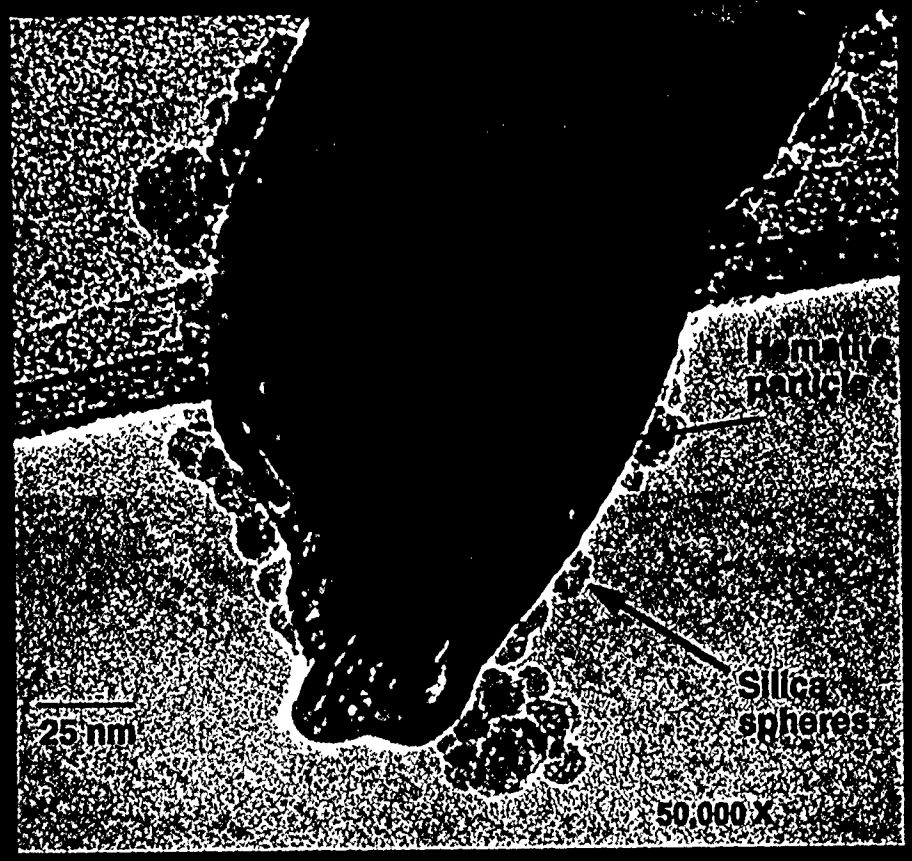

Fig. 4

Precipitated silica sticks to surface of iron oxide crystals

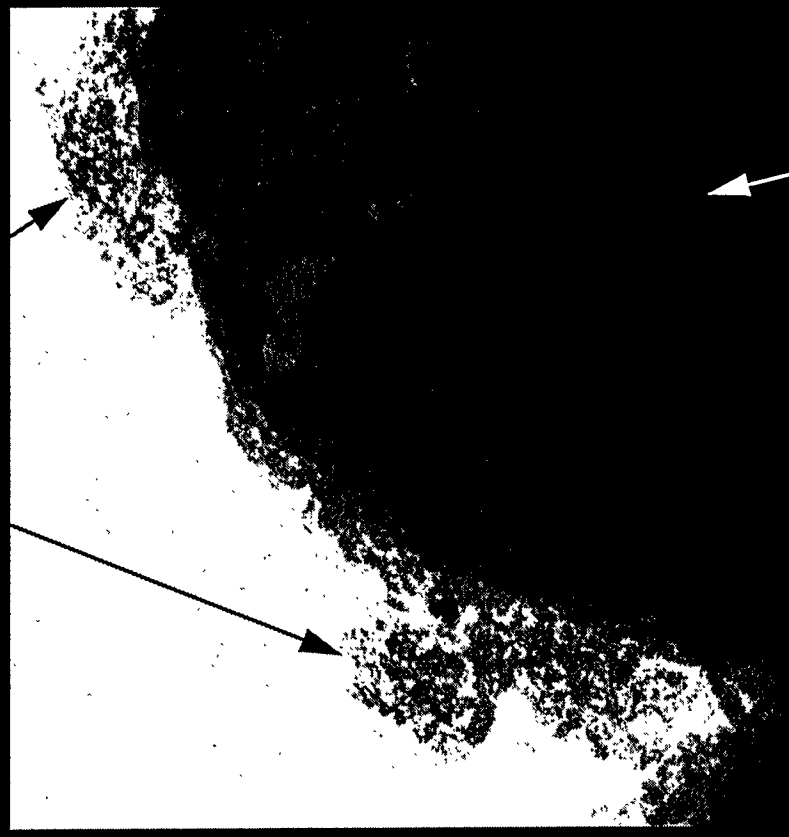

40,000X

20% molecular SiO_2 + base catalyst

Fig. 5a

Precipitated silica filling in the space between iron oxide particles

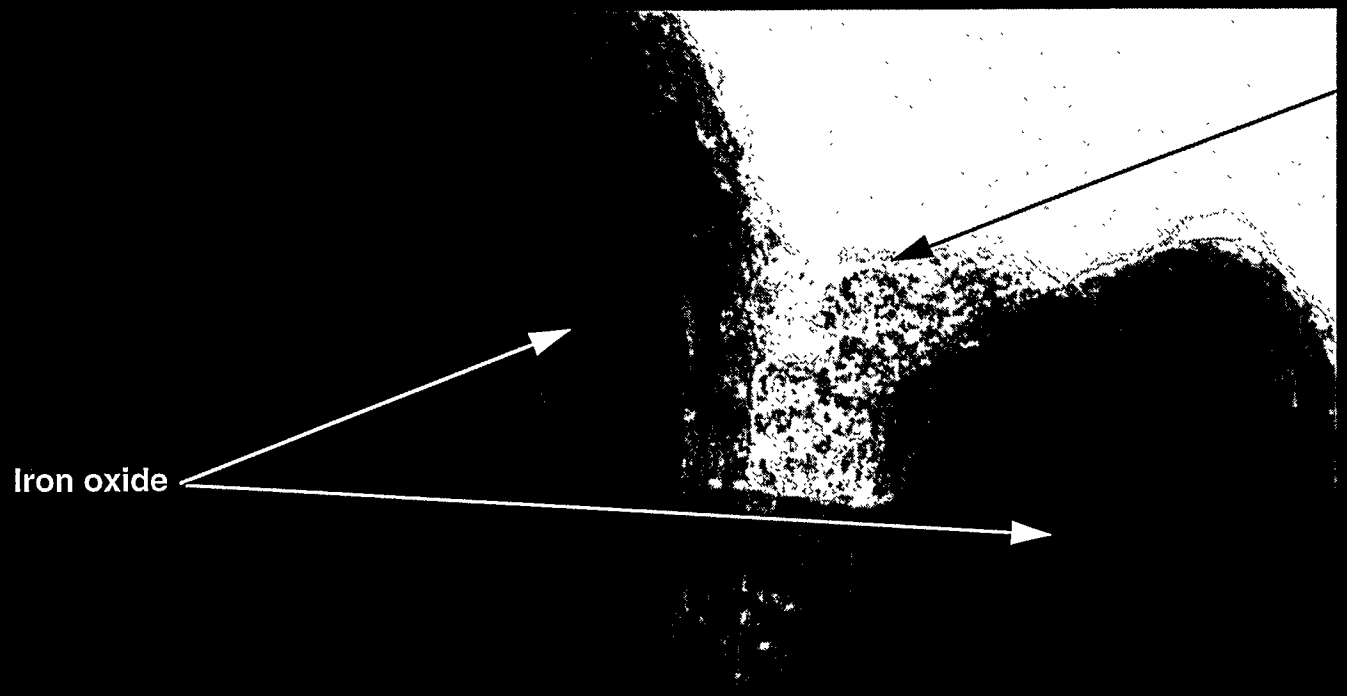

40,000X

Fig. 6

Base catalyst reduced in H_2 at 723 K

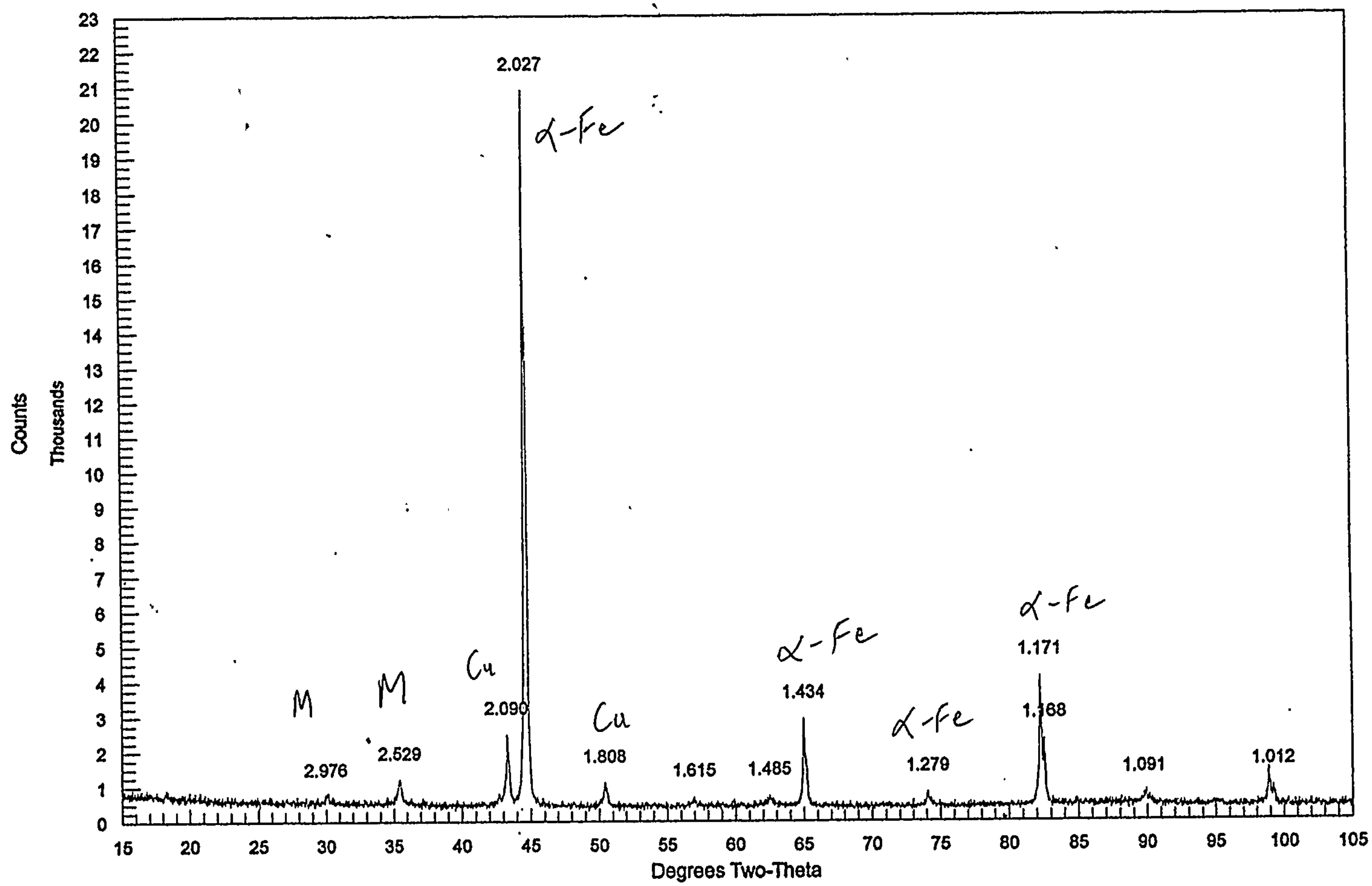

20% colloidal silica/UCI 1185-149 reduced 2 hr at 723 K

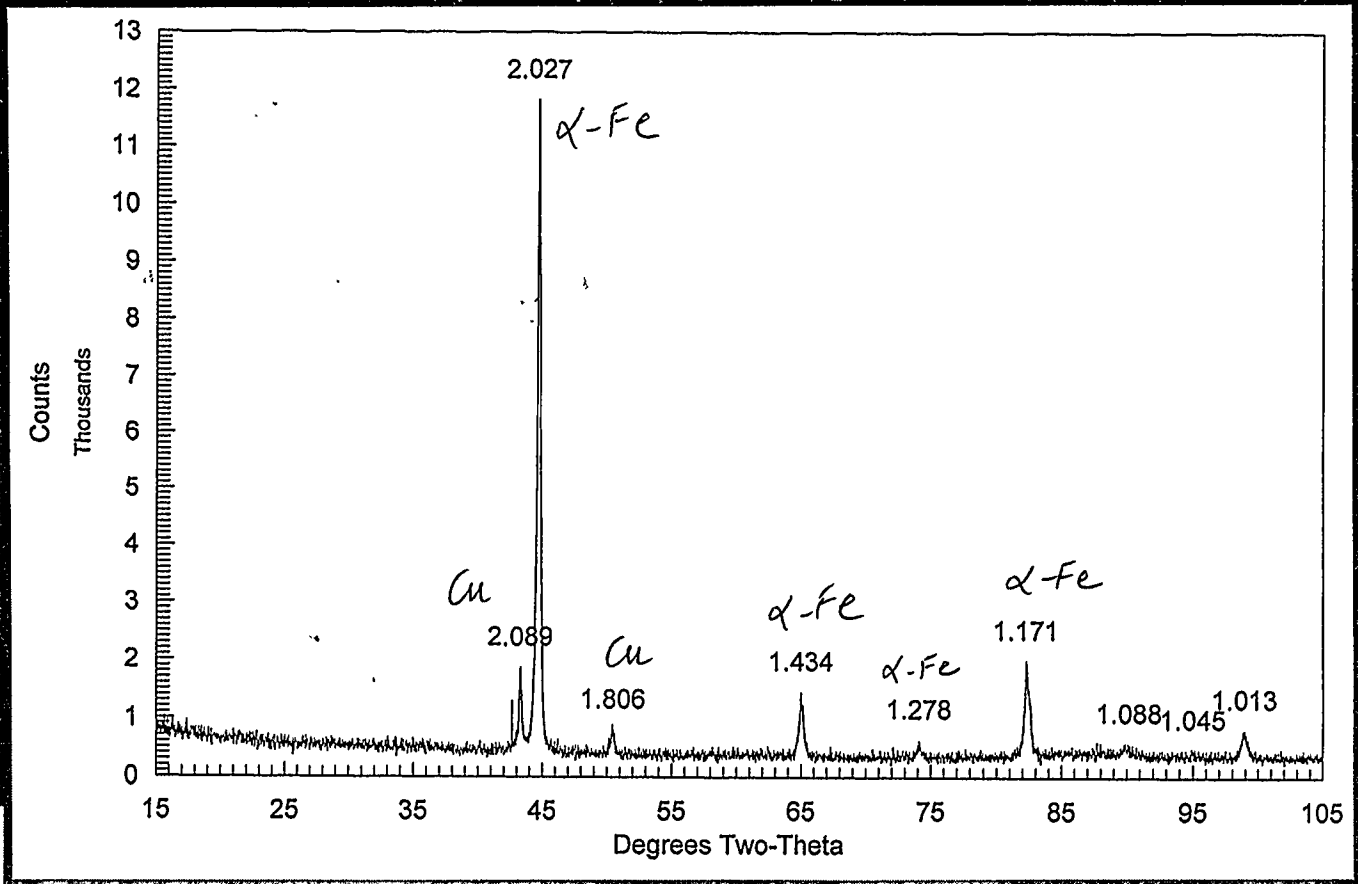

UNM

CMEC

Fig. 7

30% Fe/silica gel reduced in H_2 at 723 K

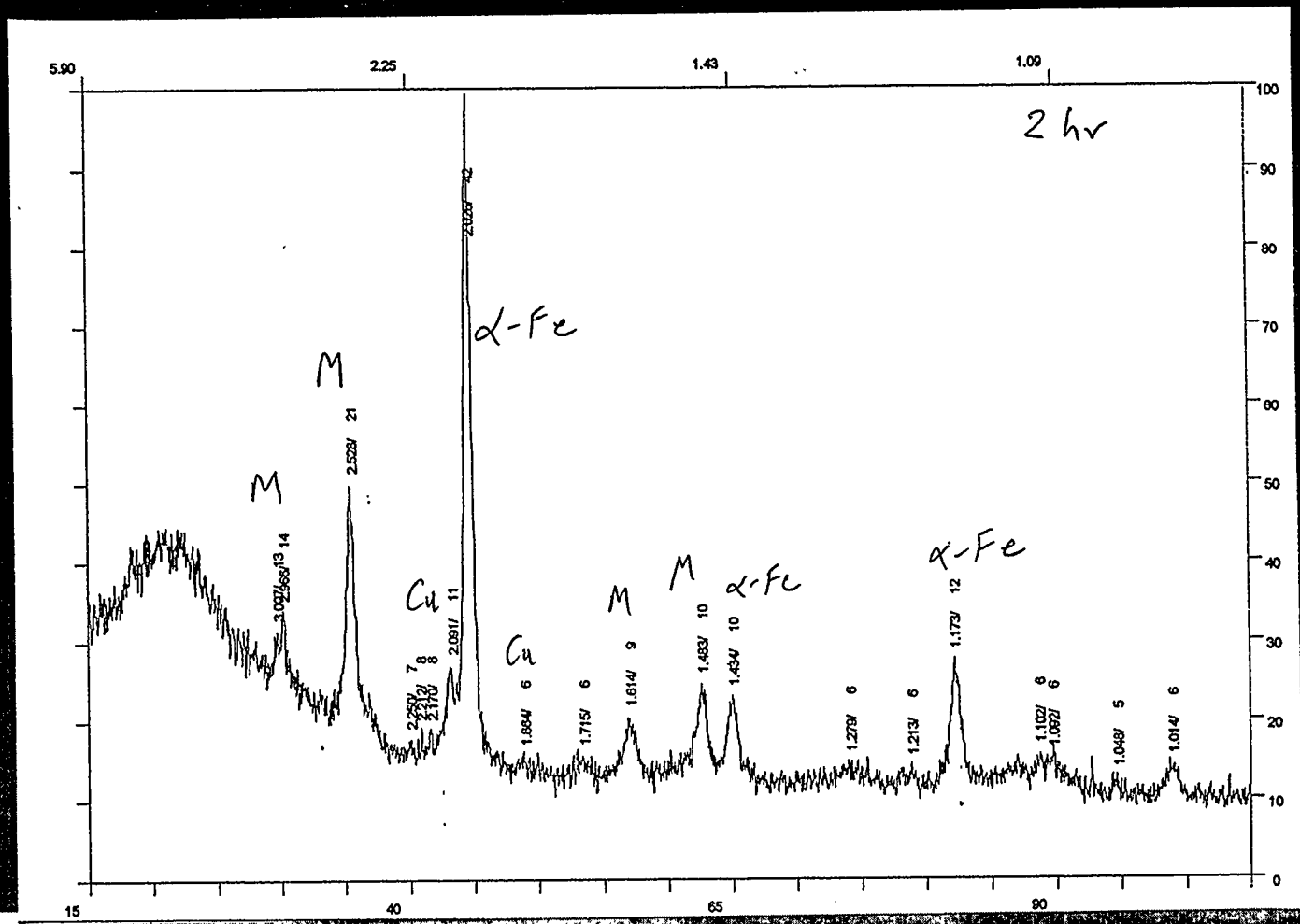

UNM

CMEC

30% Fe/SiO_2 catalyst reduced in H_2

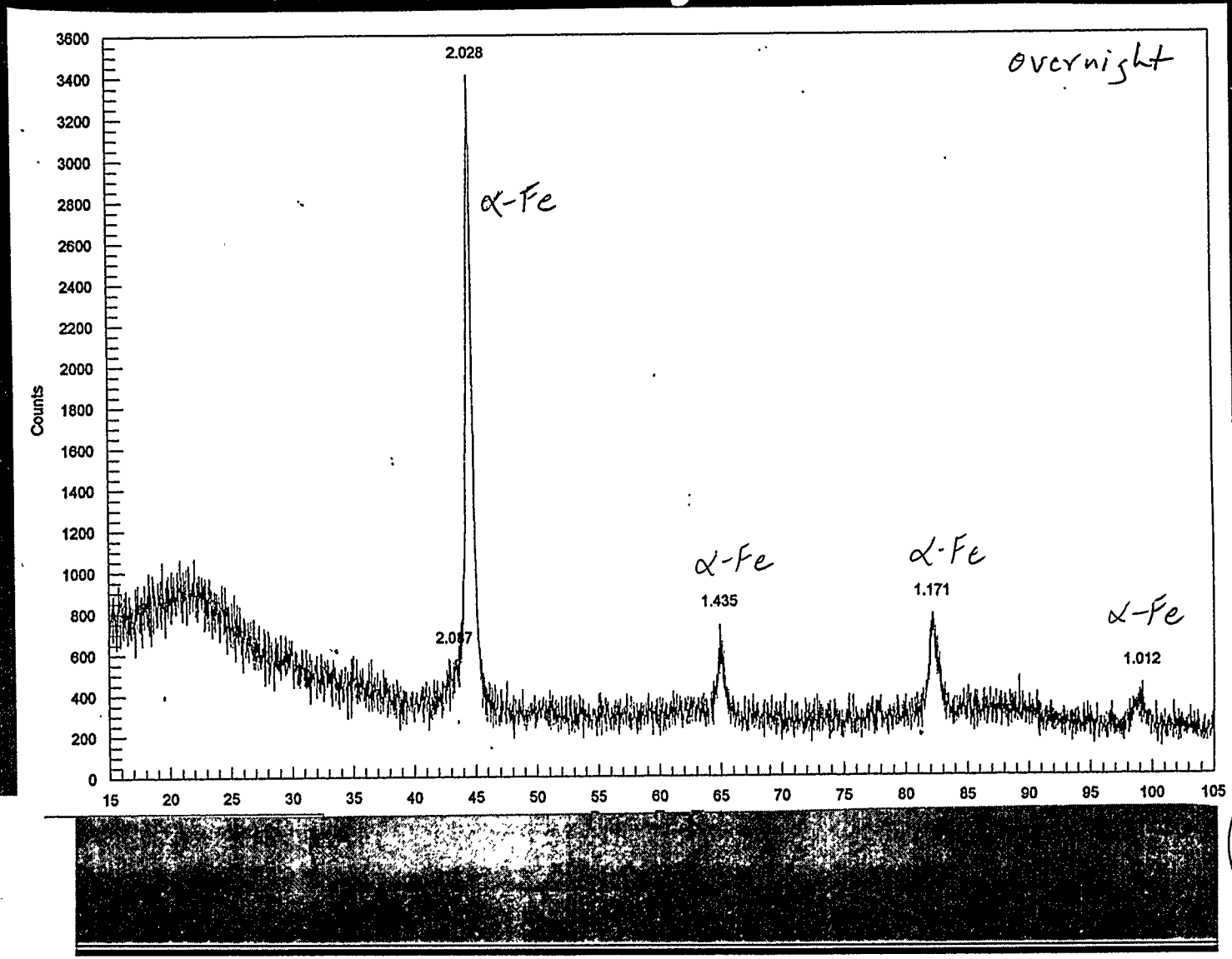

UNM

CMEC

Fig. 9

TPR RESULTS OF IRON CATALYSTS

(initial temperature 50°C, ramp 10°C/minute)

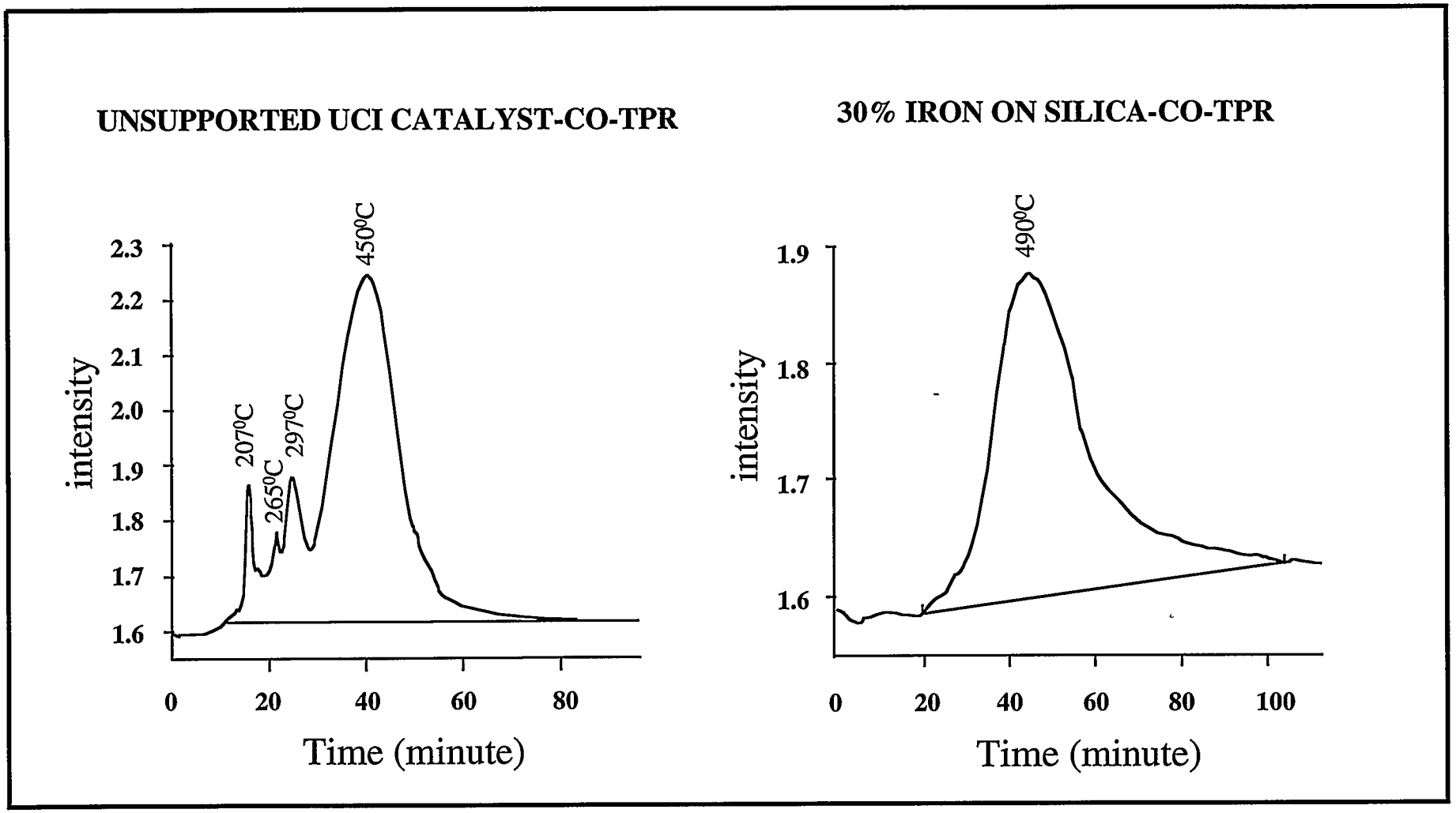

Fig. 10

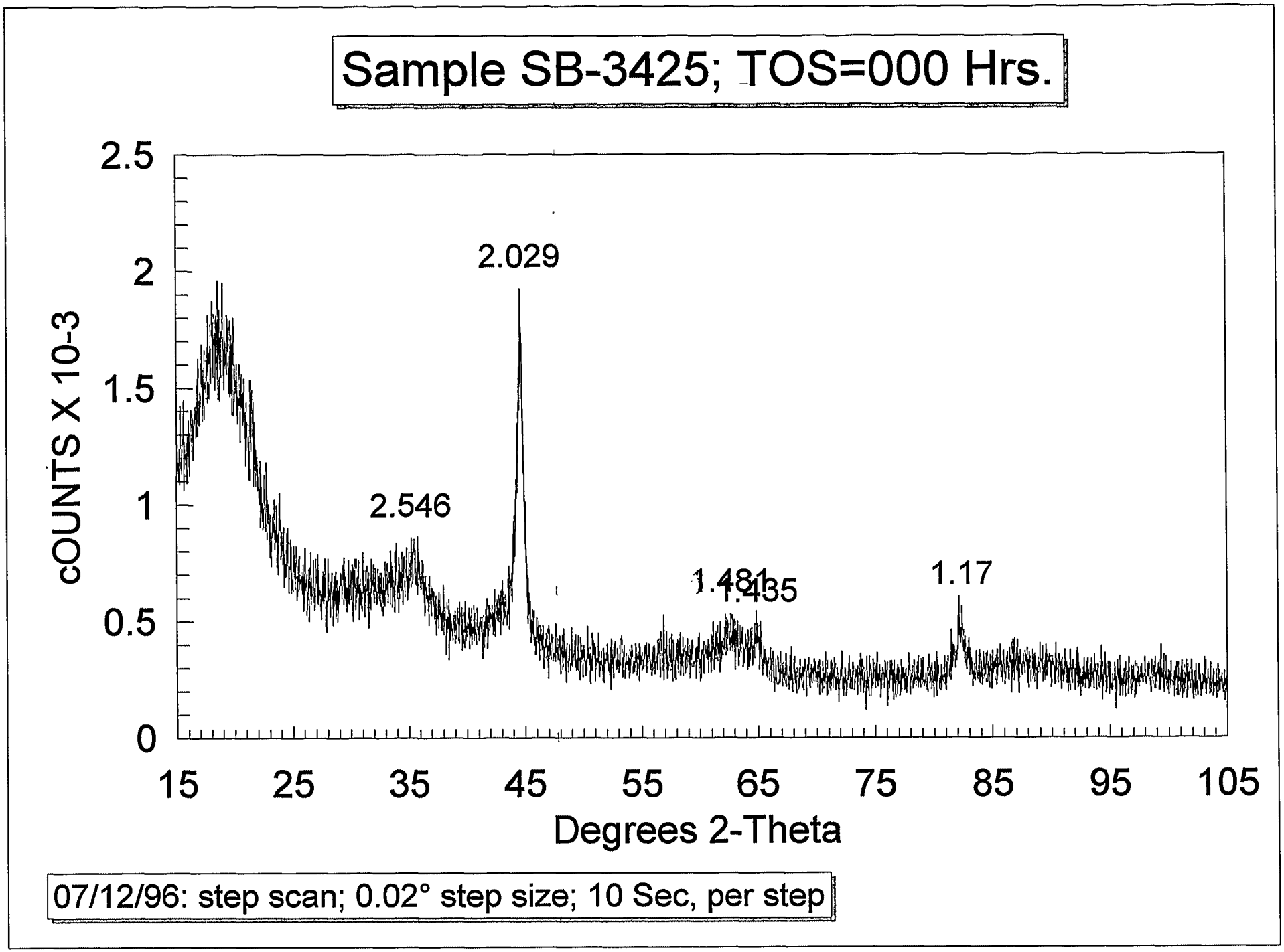
Sample SB-3425; TOS=000 Hrs.
cOUNTS X 10-3
2.5
2
1.5
1
0.5
0
2.029
2.546
1.481
1.435
1.17
15
25
35
45
55
65
75
85
95
105
Degrees 2-Theta
07/12/96: step scan; 0.02° step size; 10 Sec, per step

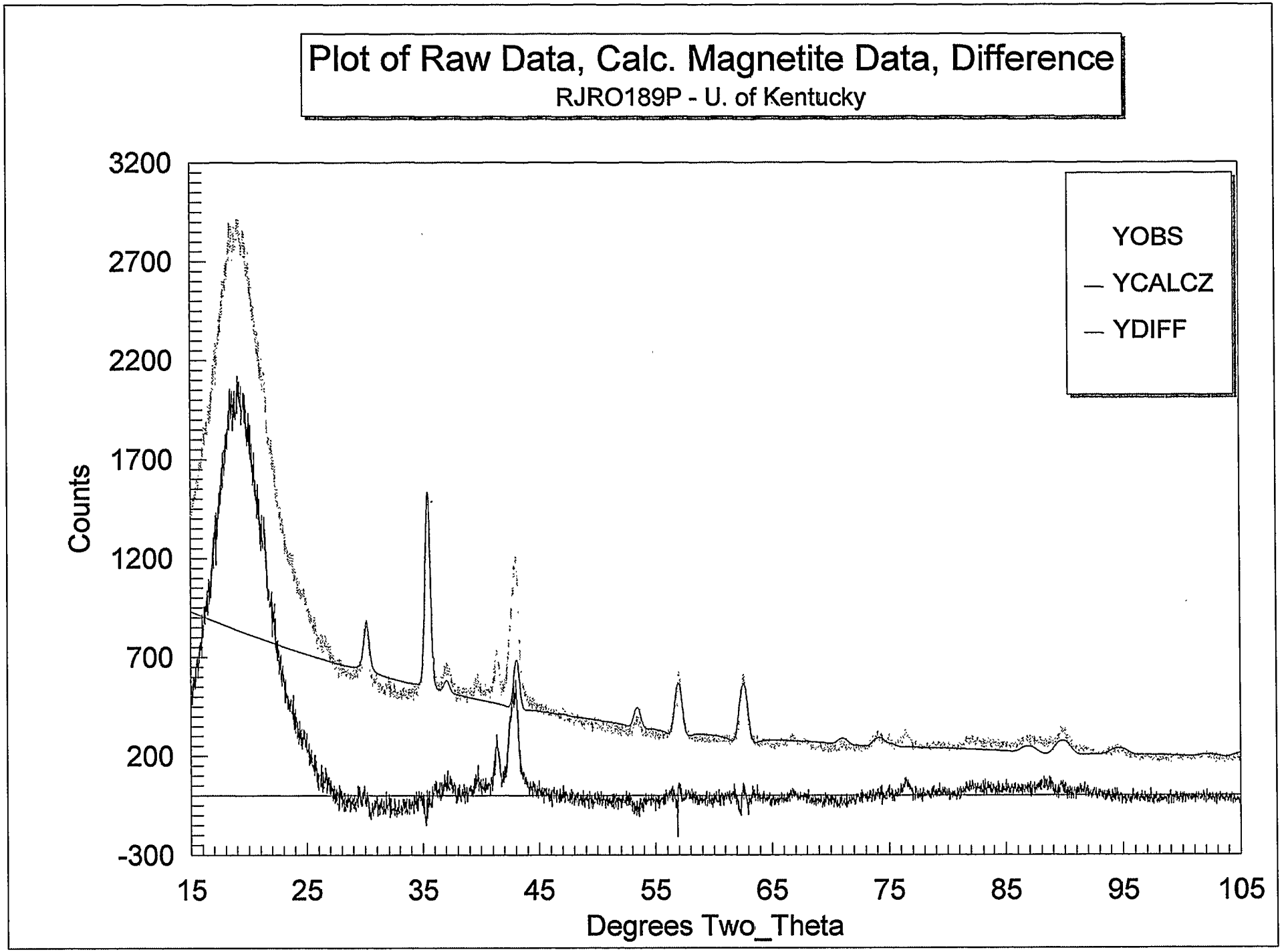
Plot of Raw Data, Calc. Magnetite Data, Difference
RJRO189P - U. of Kentucky
YOBS
YCALCZ
YDIFF
Counts
3200
2700
2200
1700
1200
700
200
-300
15
25
35
45
55
65
75
85
95
105
Degrees Two_Theta

Fig. 12

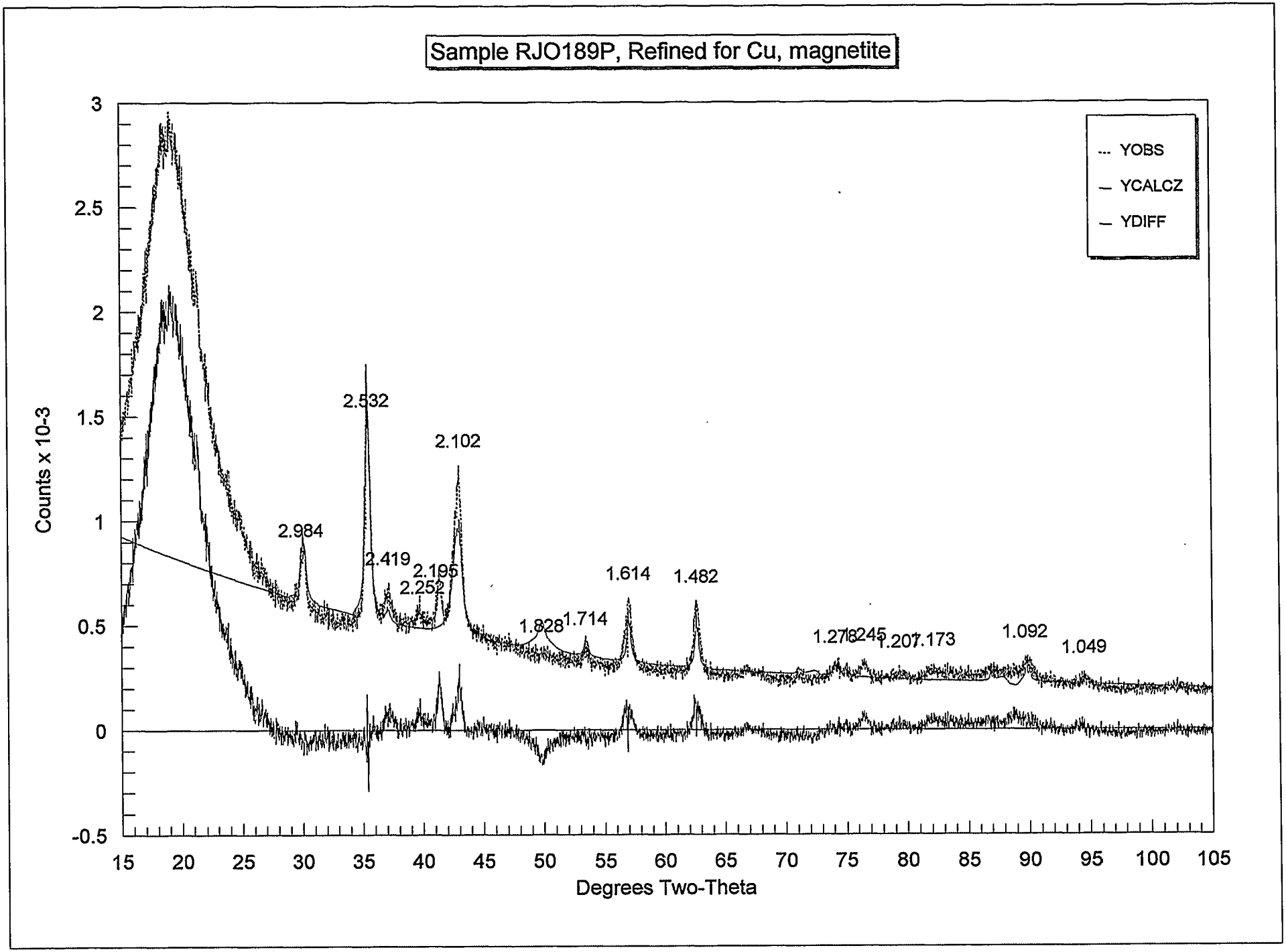
Sample RJO189P, Refined for Cu, magnetite
YOBS
YCALCZ
YDIFF
Counts x 10-3
Degrees Two-Theta
2.984
2.532
2.419
2.252
2.195
2.102
1.828
1.714
1.614
1.482
1.278
1.245
1.207
1.173
1.092
1.049

Fig. 13

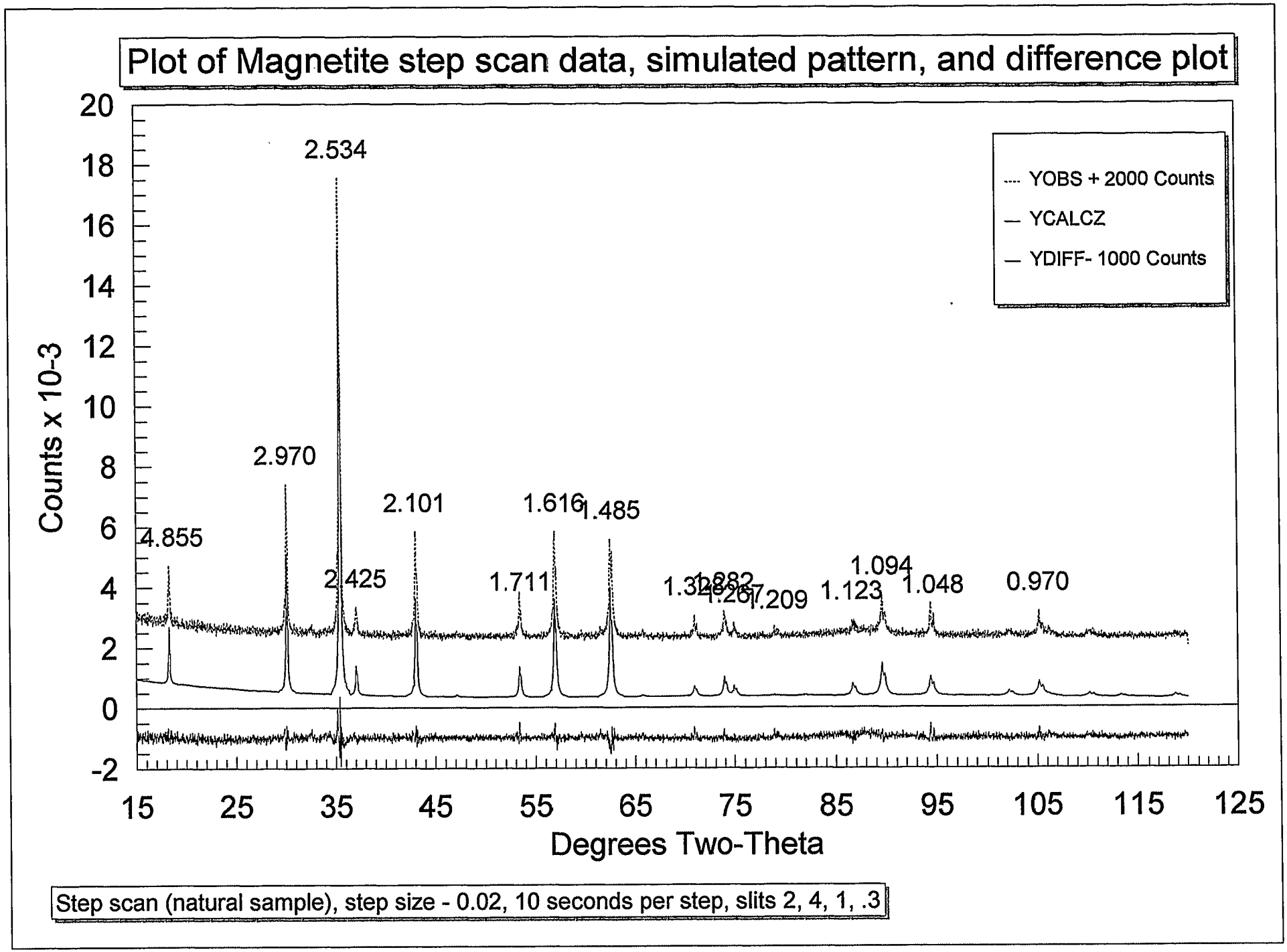
Plot of Magnetite step scan data, simulated pattern, and difference plot
YOBS + 2000 Counts
YCALCZ
YDIFF- 1000 Counts
Counts x 10-3
20
18
16
14
12
10
8
6
4
2
0
-2
2.534
2.970
2.101
1.616
1.485
4.855
2.425
1.711
1.094
1.123
1.048
0.970
15
25
35
45
55
65
75
85
95
105
115
125
Degrees Two-Theta
Step scan (natural sample), step size - 0.02, 10 seconds per step, slits 2, 4, 1, .3

Fig. 14

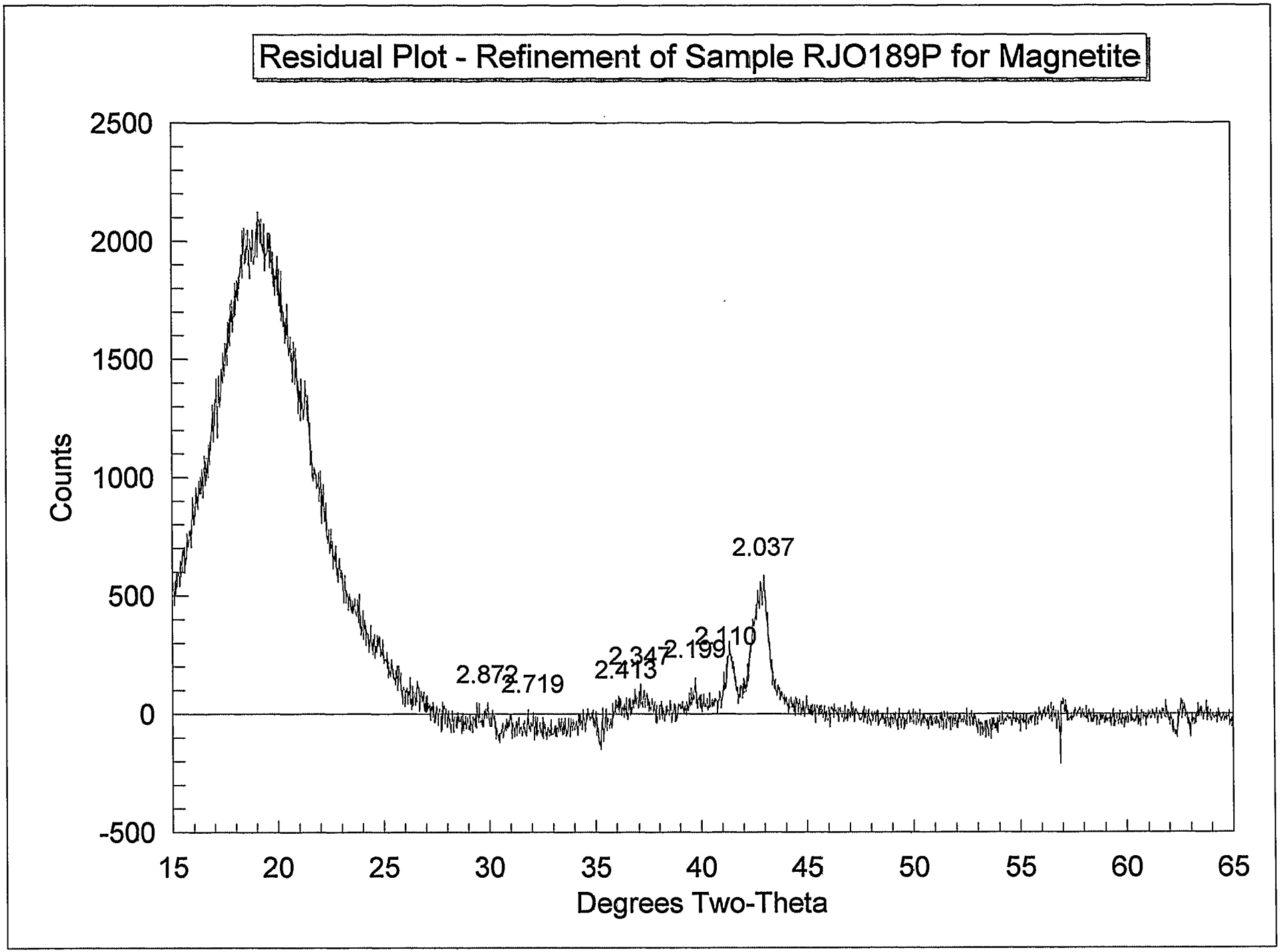
Residual Plot - Refinement of Sample RJO189P for Magnetite
2500
2000
1500
1000
500
0
-500
Counts
15
20
25
30
35
40
45
50
55
60
65
Degrees Two-Theta
2.037
2.110
2.199
2.347
2.413
2.719
2.872